



Ligand Slope, Density and Affinity Direct Cell Polarity and Migration on Molecular Gradient Surfaces

Journal:	<i>RSC Advances</i>
Manuscript ID:	RA-ART-04-2014-003795.R1
Article Type:	Paper
Date Submitted by the Author:	03-Jul-2014
Complete List of Authors:	lee, Eun-ju; UNC Chapel Hill, Chemistry chan, eugene; UNC Chapel Hill, Chemistry Luo, Wei; York University,, Chemistry Yousaf, Muhammad; York University, Centre for Research on Biomolecular Interactions, Chemistry

Cite this: DOI: 10.1039/c0xx00000x

www.rsc.org/xxxxxx

ARTICLE TYPE

Ligand Slope, Density and Affinity Direct Cell Polarity and Migration on Molecular Gradient Surfaces†

Eun-ju Lee,^a Eugene W.L. Chan,^a Wei Luo^{a,b} and Muhammad N. Yousaf^{* a,b}

Received (in XXX, XXX) Xth XXXXXXXXX 20XX, Accepted Xth XXXXXXXXX 20XX

DOI: 10.1039/b000000x

We report a combined photochemical and electrochemical approach to generate model substrates that have molecularly defined gradients of ligands for studying cell migration and polarization. Our strategy utilizes a substrate bound with a photo-labile group protected redox active molecule that can be deprotected with ultraviolet light in patterns and gradients. The unveiled redox active molecule reacts selectively with soluble oxyamine tethered ligands for molecular level tailoring of the surface. This reaction is quantitative and can be monitored and controlled with cyclic voltammetry to determine the yield of reaction and therefore also to control the precise density of ligand on the surface. The surface is also designed to be inert to non-specific protein adsorption, thus the only interaction between cell surface receptors and the material is a ligand-receptor interaction, which is critical for studying the subcellular nano-architecture within cells during cell migration. We show the subtle interplay between ligand slope, ligand density and ligand affinity that causes a cell to modulate its adhesion and migration position and behavior during directed movement. We also show single cell polarity direction on gradient patterns is controlled by the presentation of peptides on the underlying surface.

Introduction

Cell adhesion and cell migration are critically important for a number of fundamental biological processes. These diverse processes range from wound healing, metastasis, to development.¹ To initiate a complex series of events that lead to cell migration, an adherent cell requires the ability to integrate information derived from soluble growth factors with positional information gained from interactions with the extracellular matrix and with other cells.² The network to determine how a cell responds and moves involves complex signaling cascades that guide the directional and contractile functions of the cytoskeleton as well as the synthesis and release of proteases that facilitate movement through tissues.³ The biochemical events of the signaling cascades occur in a spatially and temporally coordinated manner and dynamically shape the cytoskeleton in specific sub-cellular regions.⁴ Therefore cell migration involves a precise but constantly changing subcellular nano-architecture.

While many of the key proteins and signaling molecules have been discovered that affect cell adhesion and migration, the molecular network details of how the cell interprets and processes external cues to initiate internal signaling and overall movement is largely unknown.⁵ For cell migration on an immobilized gradient (haptotaxis) the spatial presentation of ligands and the density of ligands on extracellular matrix proteins play a significant role in shaping cell function and motility.⁶ The ability to decipher the outside-in signaling, governed by the extracellular matrix proteins interactions with cell surface receptors, remains challenging and elusive due to the complexity of generating

molecularly defined model substrates to recapitulate these processes. In order to fully understand the complex signaling and cytoskeletal aspects of the cellular nano-architecture during migration, a multidisciplinary coordinated effort is required for integrating sophisticated surface chemistry to generate molecularly defined model substrates with modern cell biology and microscopy techniques.

Despite the routine use of model substrates, little is known about the mechanisms by which adherent cells initiate migration in response to signals based on changes in ligand density, ligand affinity and presentation on the surface. This is due to the difficulty in generating model substrates that are defined at the molecular level.⁷⁻⁹ Several methods have been employed to generate gradients, including polymer blend,¹⁰⁻¹⁴ laminar flow,^{15,16} photo-patterning,^{17,18} soft lithography,^{19,20} magnetic field,^{21,22} and electric field,^{23,24} but many of these strategies rely on protein adsorption in flow and have limited success in the preparation of molecularly defined *ligand gradients* for studying the influence of slope on ligand-mediated cell migration (haptotaxis). These technical challenges result in the need for model substrates that can examine how the interplay between ligand density, affinity and presentation that may influence migration. Therefore, without these model systems, many important fundamental cell motility questions remain elusive and unexplored. Herein, we report a model substrate that presents cell adhesive ligands in molecularly defined gradients. We use these surfaces to quantitatively determine how the relationship between slope, ligand density and ligand affinity affect cell polarity and cell migration.

Our model system utilizes a photochemical approach that unveils redox active surface bound groups that can selectively immobilize ligands in patterns and gradients onto electroactive self-assembled monolayers (SAMs) of alkanethiolates on gold.

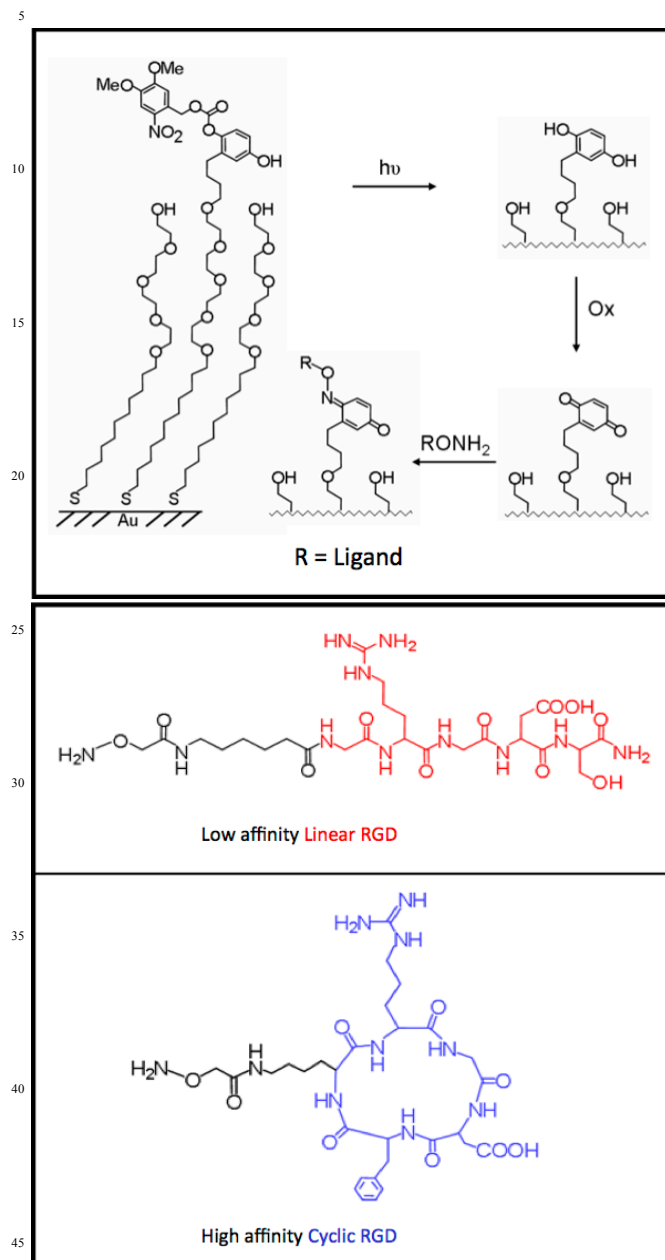


Figure 1. A photochemical strategy for patterning immobilized ligands to an electroactive self-assembled monolayer. (Top) Mixed monolayers presenting NVOC protected hydroquinone and tetra(ethylene glycol) groups are illuminated with ultraviolet light (365 nm). Photochemical deprotection of the NVOC group reveals the hydroquinone. Electrochemical oxidation of the monolayer converts the hydroquinone to the quinone. The resulting quinone monolayer can then undergo selective immobilization with soluble aminoxy terminated ligands to form a covalently bound oxime conjugate on the surface. (Bottom) The chemical structures of the low affinity Linear-RGD and high affinity Cyclic-RGD aminoxy tethered ligands for integrin cell surface receptors used for cell polarity and cell migration studies.

This approach is based on the photochemical activation of a mixed monolayer presenting nitroveratryloxycarbonyl (NVOC)

protected hydroquinone and tetra(ethylene glycol) groups (Figure 1). The NVOC protected hydroquinone permits the photo-patterning of immobilized ligands, while the tetra(ethylene glycol) provides the inert property necessary to resist the nonspecific protein adsorption. Illumination of the monolayer with a mercury lamp (365 nm) readily removes the NVOC group to reveal the hydroquinone.²⁵⁻²⁷ Subsequent electrochemical oxidation converts the hydroquinone to the corresponding reactive benzoquinone on the surface. The resulting benzoquinone monolayer can then react selectively with soluble aminoxy terminated ligands to form an oxime conjugate on the surface. This strategy possesses several unique features that are essential in the fabrication of molecularly defined gradient:

1. Ligands on the monolayer surface are presented uniformly in a homogeneous environment.²⁸
2. Ethylene glycol terminated SAMs ensure that the immobilized ligands alone mediate cell-surface interactions by preventing nonspecific protein adsorption.²⁹
3. Electroactive monolayer permits quantitative determination of ligand density by cyclic voltammetry.³⁰
4. Aminoxy tagged ligands react with the quinone form of the monolayer rapidly and in high yield at physiological pH and room temperature.³¹ This reaction can be done in complex protein mixtures and in the presence of cells to install ligands on the surface during cell migration experiments.
5. The aminoxy groups can be easily introduced into most biomolecules through straightforward solution or solid phase synthesis.³²
6. Various complex gradients of immobilized ligands can be routinely generated for patterning cell culture by using photolithographic masks (Figure 2).

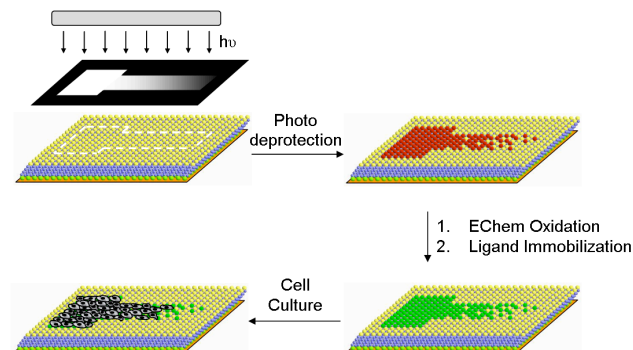


Figure 2. A strategy for generating gradients of immobilized peptide ligands for directing cell adhesion. UV illumination of the NVOC protected hydroquinone through a gradient photo mask reveals the hydroquinone in selective regions on the monolayer. Electrochemical oxidation of the hydroquinone monolayer to the quinone permits selective immobilization of soluble peptide ligands to the patterned gradient surface. Seeding cells to the resulting peptide gradient surface mediates cell attachment and migration on a molecularly defined surface.

100 Results and Discussion

To generate ligand defined gradients we prepared substrates presenting a mixed monolayer of NVOC protected hydroquinone (1%) and tetra(ethylene glycol) (99%). These substrates are initially inert to cell adhesion. After ultraviolet (UV) illumination through a photo-mask with a dumbbell gradient pattern for 30 min to selectively unveil the hydroquinone, the monolayer

substrate was then electrochemically activated by applying an oxidative potential at 750 mV for 10 s. We first immobilized soluble rhodamine oxyamine (50 mM in MeOH, 2 hrs) in order to characterize the surface modification by fluorescence microscopy.³³ Figure 3A shows the optical micrographs of various photo-masks used in generating the dumbbell gradients. Figure 3B shows fluorescent images of rhodamine oxyamine conjugated to the quinone monolayer after the photo-patterning. The immobilization of rhodamine oxyamine in selective region results in a gradient pattern identical to that of the photomask. This result confirms that the surface chemistry is compatible with the use of photomasks to generate complex ligand defined gradients on monolayer surfaces.

We next extended this photochemical strategy to pattern peptide ligands in gradients for attached cell culture to determine the relationship between slope and ligand density on cell adhesion and migration. We used solid phase peptide synthesis to generate an RGD–oxyamine ligand. The RGD peptide is found in the central cell-binding domain of fibronectin and is known to facilitate cell adhesion through cell surface integrin receptors.³⁴

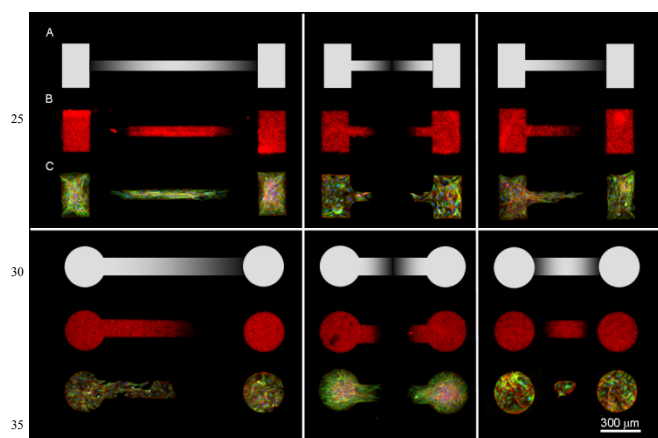


Figure 3. Representative images for the photo-patterning of fluorescent molecules and peptide ligand mediated cell attachment and migration on molecularly defined gradients. (top) (A) Optical micrographs of the photo-masks used in generating several dumbbell gradient patterns with varying slopes. (B) Fluorescent images of surface immobilized rhodamine oxyamine after the photo-patterning. (C) Fluorescent images of Swiss 3T3 fibroblasts on linear-RGD ligand gradients. (bottom) Another group of experiment based on different pattern shape. Cells were allowed to attach, proliferate and migrate on the gradients until they stopped moving and then fixed and stained for actin (red), tubulin (green), and DNA (blue).

For the cell migration studies, we prepared mixed monolayer presenting 1% NVOC protected hydroquinone and 99% tetra(ethylene glycol) groups. Illumination through various dumbbell gradient photo-mask patterns followed by electrochemical oxidation converted the surface to gradient regions of reactive benzoquinone monolayer for subsequent immobilization of oxyamine tethered ligands. Selective immobilization of soluble oxyamine tagged RGD peptide (30 mM in PBS, 4 hrs) to the benzoquinone monolayer generated the peptide gradients on the surface. Addition of Swiss 3T3 fibroblasts resulted in cell attachment to the dumbbell gradient patterns. The cells initially attached to the higher peptide density

regions of the gradients. The monolayer substrates were then placed in serum containing media to permit cell growth and migration. The cells proliferated and migrated down the gradients and then stopped at their final positions due to the lack of peptide ligand density to support further adhesion and migration (experiment stopped after 72 hours, although no further migration occurred beyond 48 hours on the gradients). As controls to separate the role of cell proliferation and migration, all experiments were repeated in the absence of serum (to minimize cell proliferation) and the cells stopped at approximately the exact same locations on the various gradients. Furthermore the experiments were repeated in serum in the presence of 5 $\mu\text{g}/\text{ml}$ of mitomycin C (this molecule inhibits cell proliferation but does not affect cell migration at this concentration level) and the cells again stopped at the same ligand density on the peptide gradients. Figure 3C shows representative fluorescent images of fixed cells on various RGD immobilized gradients. The images show that the adherent cells are completely confined within the patterns demonstrating that the use of UV light and electrochemical oxidation did not damage the monolayer surfaces which would lead to nonspecific cell attachment. These results show that cell attachment on the peptide gradients clearly depends on the density and slope of immobilized ligands. As the peptide density decreases along the gradient a minimum density is reached below which cell migration and adhesion cannot be supported. Finally, the relative positions at which cells attached along both sides of the gradients are remarkably similar on most of the symmetrical patterns. This result implies that both the photo-patterning and the surface chemistry that control the peptide immobilization are well defined on these gradient surfaces. As controls we immobilized a scrambled peptide-oxyamine (GRD-ONH₂) to the gradient surfaces and no cells attached. To show biospecific cell attachment, we also added a soluble competing RGD peptide (1 mM for 30 min) to the media and all the adhered cells on gradients detached indicating a ligand-receptor interaction between the cells and the surface.

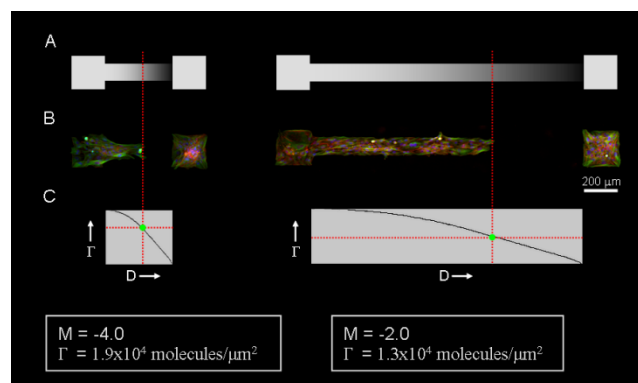


Figure 4. Analysis of the slopes and ligand densities along various linear-RGD ligand gradients to determine their influence on cell adhesion and migration. (A) Optical micrographs of the different gradient photo-masks. (B) Fluorescent images of fixed and stained cells after they stopped migrating on peptide gradients of various slopes (M). (C) A plot of ligand density (Γ) versus distance (D) along the gradient was generated from the photo-mask shown in 4A using ImageJ. The plot is aligned perpendicularly with the patterned cells in order to determine the minimum density required to support cell migration on a peptide gradient.

We next studied whether ligand density alone or the combination of slope and ligand density governs cell migration. If cell migration is solely based on the underlying ligand density, we expect that the adherent cells would migrate down the gradient until the ligand density is insufficient for supporting cell attachment. The minimum ligand density for cell attachment over long periods of time (equilibrium position) would therefore be similar on all the gradients irrespective of slope. In order to determine the peptide density for cell attachment along the gradient, we used an image analyzing software (ImageJ) to first obtain a density profile of the gradient based on the pixel intensity of the photomask and the corresponding fluorescent micrographs of rhodamine immobilization. The slope profile for the photomask and the corresponding rhodamine immobilized surface are approximately identical (Supplementary Data). Figure 4A shows the optical micrographs of the photomasks. Figure 4B shows the fluorescent images of attached cell culture on RGD immobilized dumbbell gradients generated by the photo-mask shown in 4A. Figure 4C shows a plot for the relative density with respect to the distance along the gradient generated from ImageJ. To extrapolate the density along the gradient from this plot, we assume that the maximum peptide density (Γ) is 2.7×10^4 molecules/ μm^2 based on 1% NVOC hydroquinone monolayer that has been completely modified to the peptide ligand on the surface. The ligand density at 1% NVOC hydroquinone was determined based on integration of the area under the oxidative or reductive waves corresponding to the hydroquinone monolayer after the photo-deprotection of monolayer presenting only the NVOC hydroquinone groups. The value obtained was 4.5×10^{-20} mol/ μm^2 (2.7×10^4 molecules/ μm^2). By aligning the density plot with the patterned cells, we determine the minimum ligand density for supporting cell adhesion along the gradient. Interestingly, our data show that the minimum density varies on each gradient. This result suggests that cell migration is not solely dependent on density of surface-bound ligands.

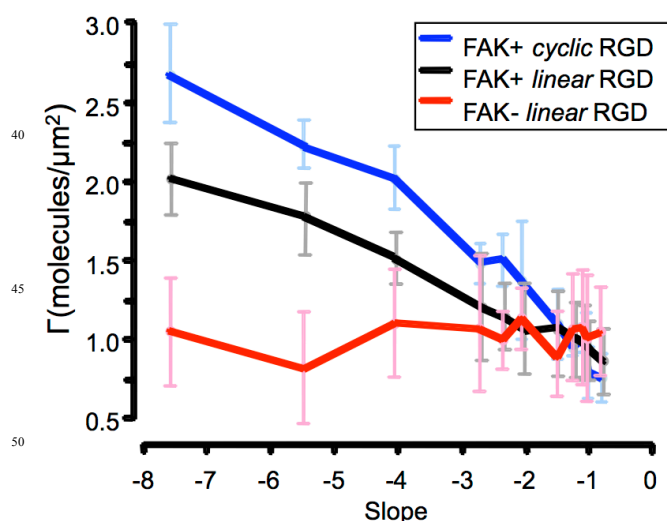


Figure 5. Relationship between ligand density, ligand affinity and gradient slope for two different cell-types. Each data point represents an average from four separate sets of experiments. The cells over time position themselves to varying ligand density depending on the slope of the gradient. Mouse embryonic fibroblasts (FAK+) cells re-adjust their position depending on the slope and affinity of peptide ligand while FAK-

null fibroblasts (FAK-) which have a focal adhesion defect, position themselves to the same density irrespective of slope and ligand affinity.

We also examined how the slope of ligand presentation may play a role in affecting how, where and when cells migrate. By coaxing the cells to migrate from higher density ligand toward lower density on gradients with different slopes, we can establish whether there is a correlation between the slopes and minimum ligand density for cell attachment on the gradient. For these experiments, we generated gradient patterns with different slopes on a photo-mask by systematically varying the length of the gradients. We use arbitrary values for both the density and distance along the gradient obtained from ImageJ to calculate the slopes. We then prepared the peptide gradients with slopes ranging from -1 (the shallowest) to -8 (the steepest) for cell culture. Figure 5 shows a plot for the dependence of minimum ligand density for cell attachment of various cell-types on the slopes of gradients. The data show that Swiss 3T3 fibroblasts (FAK+/+) on steeper slopes terminate migration at higher peptide density when compared to the cells on shallower slopes. This result suggests cells that migrate on linear-RGD defined gradients can sense and therefore respond accordingly to the subtle changes due to ligand presentation on the surface. To establish a connection between the underlying gradient and intracellular protein activation, we repeated the migration experiment using focal adhesion kinase-null (FAK-/-) cells derived from mouse embryos. FAK is a non-receptor protein tyrosine kinase localized at focal adhesions and is essential for integrin-stimulated cell migration.³⁵ Focal adhesions are sites found at the plasma membrane that mechanically link and anchor the cytoskeleton to integrin clusters and the extracellular matrix. These are also centers for complex biochemical signaling for many pathways critical for cell function.³⁶ Deletion of FAK expression has been shown to impair cell migration.³⁷ Unlike the Swiss 3T3 fibroblasts, we found that FAK-null cells on linear-RGD gradients migrate to the same ligand density at equilibrium regardless of the slopes (red line). As a control, we repeated the experiments using wild-type (FAK+/+) cells, and observed that FAK+/+ cells exhibit similar dependence of ligand density on the slopes as the Swiss fibroblasts (black line). This result suggests that focal adhesion kinase may be critical in sensing ligand presentation during cell migration. As further evidence that ligand affinity also plays a role in cell migration, we immobilized a cyclic-RGD peptide to the surface and compared the cell migration equilibrium positions with linear RGD peptide gradients (blue line). We found at steeper slopes the FAK+/+ cells required more cyclic-RGD ligand density than for linear-RGD. This result implies for the first time that although the affinity for cyclic RGD is greater than that for linear RGD, the steepness of the gradient across a cell length alters the requirements for ligand density for cell migration. These are the first results to compare ligand affinity, density and slope for cell migration studies and are significant to fundamental cell biology and cancer metastasis studies.

Figure 6 shows an illustration summarizing the data obtained from Figure 5 for linear-RGD immobilized surfaces. Upon seeding of FAK+/+ and FAK-/- cells to the surface, both cell lines initially attached to the region of the gradient that presents the highest linear-RGD ligand density. The cells migrated and

proliferated at this high density region until they became contact inhibited and then started to migrate down the gradient. For the FAK+/+ cells there is no impairment of their cell migration machinery and therefore are able to sense the change in ligand density across their length and tune their position along the gradient.

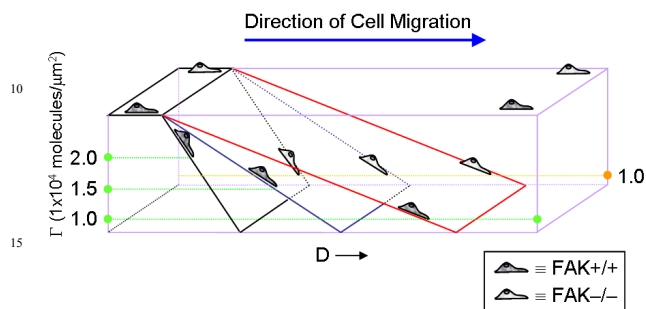


Figure 6. An illustration describing the dependence of ligand density (linear RGD) on the slopes of gradients for FAK+/+ cells and FAK-/- cells. The cells initially attach to the higher density region of the gradient pattern (left) and proliferate and migrate down various slopes to their final equilibrium position over time. The migration of FAK+/+ cells is governed by a combination of ligand density and slope of the gradient. The cells migrate to different ligand density along the gradient and therefore are able to modulate their position according to the steepness of the slope. In contrast, the migration and final position of FAK-/- cells depends only on the ligand density. These cells move to the same ligand density regardless of slope.

By presenting various slope planes we were able to show that FAK+/+ cells require higher ligand density to support adhesion on steep gradients and lower ligand density on shallow gradients. In stark contrast FAK-/- cells that have their focal adhesions severely compromised due to the absence of the critical focal adhesion kinase were unable to sense the peptide gradient and positioned themselves to the same density irrespective of slope. Further analysis of the underlying gradient shows the percent drop-off in ligand density along a cell length ranges from 55% for the steepest gradient (-8) to 5% for the shallowest gradient (-1) for a 100 μm length cell. For the FAK+/+ cells the severity of the change in ligand density at steep slopes induce the cells to require more ligands to support adhesion. On shallow slopes the cells are able to migrate to regions with much lower ligand density indicating fewer ligands are required to support cell function and adhesion. Interestingly, the FAK+/+ cells were able to migrate towards much lower ligand densities when presented on a shallow gradient than would support their initial attachment in a standard adhesion assay. These results show quantitatively that a cell has the ability to modulate its behavior by precisely determining the change in ligand density and affinity from its leading to trailing edge. The ability for a cell to modulate its internal nano-architecture to sense and respond to the surface environment is critical for regulating directional movement.

We next extend this methodology to study single cell polarization. The ability for a cell to polarize and therefore generate asymmetry within itself due to external factors is critical for a range of biological processes.³⁸ The role of the underlying adhesive environment and cell-cell interactions is critical to establish cell polarity but is not well understood.

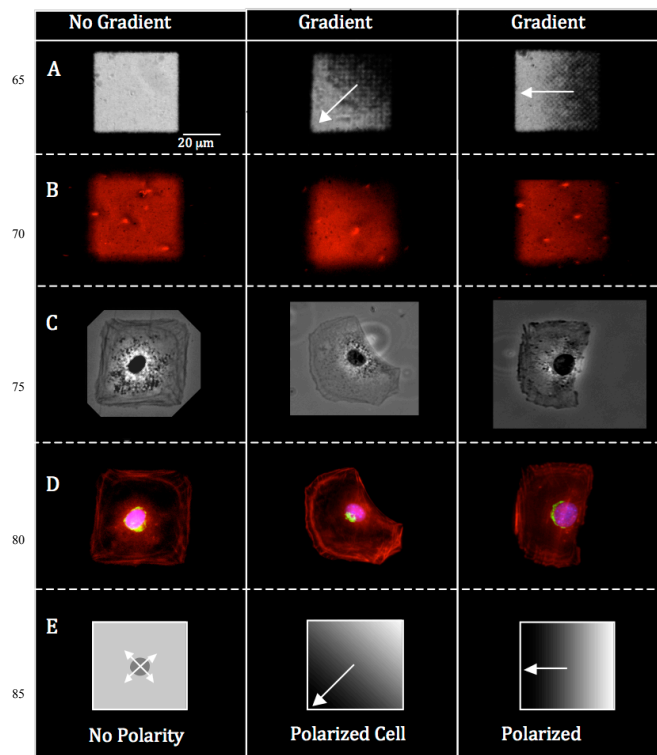


Figure 7. Single cell fluorescent images of polarized cells on small pattern linear-RGD immobilized gradients. (A) Optical micrograph of the microfiche photo-mask used for the photo-deprotection of the NVOC-hydroquinone to generate a surface gradient. (B) Fluorescent image of immobilized rhodamine-oxyamine to the surface generated by the gradient photo-mask. This fluorescent gradient is used to show that the ligands immobilized on the surface have the same slope as the photomask. (C) Representative phase contrast micrographs of 3T3 Swiss Albino mouse fibroblast adhered to non-gradient and gradient patterns of immobilized linear RGD peptide. (D) Fluorescent images of the cells stained for actin (red) nuclei (blue) and Golgi apparatus (green) to determine the direction of cell polarity. The vector between the concentrated Golgi with respect to the nucleus and centrosome determine directional cell polarity. (E) For the non-gradient pattern (left column), the diffuse distribution of the Golgi surrounding the nucleus indicates the cell is not polarized. For cells on the gradient surfaces (center and right columns) the net vector points consistently towards the higher density adhesive regions. These results show the underlying peptide ligand gradient directs cell polarization.

In order to study the underlying surface chemistry requirements for cell polarity, we confined cells to small pattern gradients where the cells attach and become polarized due to the underlying linear-RGD ligand gradient but are not able to migrate (Figure 7).³⁹ The most conclusive method to determine cell polarity is to measure the vector between the cell nucleus, concentrated Golgi and centrosome. The polarity of a cell can be experimentally observed and measured through the systematic reorientation and alignment of these organelles, which can be visualized using fluorescent dyes to map the direction of polarity.⁴⁰ Giantin, a protein found in the membrane of the Golgi apparatus cisternae, was chosen as a marker for that organelle.⁴¹ As can be seen in the series of representative fluorescent micrographs in Figure 7, the adherent cells adopt a morphology

in which the nucleus is located approximately in the center of the cell. By determining the alignment vector of the Golgi apparatus relative to the nucleus and centrosome, we found no consistent directional polarity on the non-gradient square patterns for many cells ($n = 68$). In fact, almost all cells had a diffuse Golgi around the nucleus, a strong indicator of no polarity. For gradient square patterns (Figure 7, middle and right columns) the cells consistently polarize towards the higher density linear-RGD regions as shown by the relative positions of the nucleus and the concentrated Golgi apparatus ($n=82$). Statistical analysis of the three patterns (Figure 7E) show the polarity vector for cells on the gradients is directed to the higher density and therefore more adhesive region of the pattern, whereas there is no net vector in any direction on the non-gradient or uniform square pattern (Figure 7E). These results clearly show in the absence of cell-cell interactions a cell can be directly influenced by its surface gradient environment to polarize towards the higher density peptide ligands. Interestingly, when a higher affinity ligand (cyclic RGD) is immobilized to the gradient patterns no net directional polarity occurred. We hypothesize the affinity of the ligand and the spatial presentation of the ligands combine to govern the ability for the cell to polarize. These results show the underlying gradient directly determines cell polarization using the acceptable polarity measure of the vector between the nucleus, Golgi and centrosome. The combined photochemical and electroactive surface strategy may be used to determine single cell polarity on a variety of ligand immobilized surfaces and how cell geometry may influence the requirements for adhesion and migration on molecularly defined gradients.

Methods

All the solvents for the synthesis were HPLC grade. THF was distilled from sodium benzophenone under nitrogen before use. Absolute ethanol was purchased from Aaper Alcohol Chemical Company. Flash chromatography was carried out using silica gel (230–400 mesh). All amino acids and resin were purchased from Anaspec, Inc. (La Jolla, CA). All reagents were purchased from Aldrich and used as received. All reagents used in cell culture were obtained from Gibco BRL. 3T3-Swiss albino fibroblasts, FAK^{+/+} and FAK^{-/-} mouse embryonic fibroblasts (MEF) were purchased from ATCC.

Synthesis of Alkanethiolates

NVOC protected hydroquinone tetra(ethylene glycol) alkanethiol, tetra(ethylene glycol) alkanethiol, and rhodamine oxyamine were prepared as previously described.^{28,32}

Solid-Phase Peptide Synthesis

All peptides were synthesized by automated solid phase peptide synthesis using the CS136XT Peptide Synthesizer (CS Bio Co., Menlo Park, CA).

Linear RGD. Fmoc (9-fluorenylmethoxycarbonyl)-protected amino acids were used on Fmoc-Ser(tBu)-Rink Amide-MBHA resin. Synthesized peptide was cleaved from the resin by agitating in a solution of trifluoroacetic acid (TFA):water:triisopropylsilane (95:2.5:2.5) for 3 hours. TFA was evaporated and the cleaved peptide was precipitated in cold diethyl ether. The water-soluble

peptide was extracted with water and lyophilized. Mass spectral data confirmed the peptide product. MS (ESI) (m/z): $[M+H]^+$ calculated for linear RGD-oxyamine ($C_{25}H_{45}N_{11}O_{11}$), 676.69; found, 676.5. $[M+H]^+$ calculated for control scrambled peptide, GRD-oxyamine ($C_{25}H_{45}N_{11}O_{11}$), 676.69; found, 676.4. $[M+H]^+$ calculated for control soluble peptide RGD ($C_{17}H_{31}N_9O_8$), 490.48; found, 490.3.

Cyclic RGD. The peptide DfKRG was synthesized using H-Gly-OH preloaded 2-chlorotrityl resin. The mixture of acetic acid:trifluoroethanol:dichloromethylene (1:1:3) was added for cleavage. The resulted peptide was dissolved in DMF and added with N, N-diisopropylethylamine (DIEA) and PyBOP. The reaction was stirred for 12 hours and the solvent was removed in vacuum. The resulted cyclic peptide was treated with TFA:water:triisopropylsilane (95:2.5:2.5) for 3 hours and precipitated in diethyl ether. To introduce the oxyamine group on Lys side chain, the peptide was treated with BOC-aminoxy acetic acid, PyBOP and DIEA in DMF for 10 hours. After removing DMF, the peptide was added with TFA for 1 hour and precipitated in diethyl ether. The sample was dissolved in water and purified by HPLC (Waters). MS (ESI) (m/z): $[M+H]^+$ calculated for cyclic RGD-oxyamine ($C_{29}H_{44}N_{10}O_9$), 677.72; found, 677.4.

Microscopy of Attached Cell Culture

Adherent cells were fixed in 3.7% paraformaldehyde in phosphate buffer saline (PBS) for ten minutes and then permeabilized with 0.1% Triton X in PBS (PBST) for ten minutes. Cells were then stained with anti-tubulin (1:1000) in PBS containing 10% goat serum for one hour, followed by Alexa 488-conjugated goat anti-mouse IgG (1:100 in PBST), phalloidin-tetramethylrhodamine B isothiocyanate (1:50 in PBST), and DAPI (1:300 in PBST) for one hour. Substrates were rinsed with deionized water before mounted onto glass cover slips for microscopy. For single cell polarity studies on surface gradients, a combination of fluorescent dyes were used to visualize the fibroblasts: DAPI (4', 6-diamidino-2-phenylindole dihydrochloride for the nucleus, Sigma, St. Louis, MO), phalloidin-tetramethylrhodamine B isothiocyanate (Sigma, St. Louis, MO) for F-actin cytoskeleton, anti-giantin (Covance Research Products, Berkeley, CA) with a fluorescent tagged secondary antibody (fluorescein conjugated goat anti-rabbit IgG, Jackson ImmunoResearch Laboratories, Inc., West Grove, PA) targeting the Golgi apparatus, and mouse monoclonal anti-gamma tubulin (Sigma) to track centrosome position. All optical and fluorescent micrographs were imaged using a Nikon inverted microscope (model TE2000-E). All images were captured and processed by MetaMorph.

Preparation of Monolayers

All gold substrates were prepared by electron-beam deposition of titanium (5 nm) and then gold (15 nm) on glass cover slips (75 mm x 25 mm). All gold coated glass substrates were cut into 1 cm² pieces and washed with absolute ethanol. The substrates were immersed in an ethanolic solution containing the alkanethiolates (1 mM) for 12 hours, and then cleaned with ethanol prior to each experiment.

Electrochemical Measurements

All electrochemical experiments were performed using a Bioanalytical Systems CV-100W potentiostat. Electrochemical

oxidation of the monolayer was performed by applying an oxidative potential at 750 mV for 10 s in 1M HClO₄, using a platinum wire as the counter electrode, Ag/AgCl as reference, and the gold/SAM substrate as the working electrode.

Fabrication of Photomasks.

The photopatterns were designed and drawn in PowerPoint. The patterns were then reduced 25 times and printed onto microfiches.

Photochemical Deprotection of Substrates

A substrate presenting NVOC protected hydroquinone and tetra(ethylene glycol) groups (1:1) was illuminated with ultraviolet light (100W Hg lamp, Nikon) filtered through a band-pass filter (365 nm) for 30 minutes to ensure complete deprotection of the NVOC groups.

Photopatterning of Peptide Ligands

UV illumination of a substrate presenting NVOC protected hydroquinone and tetra(ethylene glycol) groups (1:99) through a photomask for 30 minutes removed the NVOC groups. The substrate was then oxidized electrochemically at 750 mV for 10 s to convert the hydroquinone to the quinone. A RGD oxyamine solution (50 mM in PBS) was added to the substrate for four hours to ensure complete immobilization of the peptide ligands. The substrate was then clean with water and dried before using for cell culture.

Cell Culture

Swiss 3T3 fibroblasts, FAK^{+/+} and FAK^{-/-} MEF were cultured in Dulbecco's Modified Eagle Medium (Gibco) supplemented with 10% calf bovine serum and penicillin/streptomycin. Cells were removed with a solution of 0.05% trypsin/0.53 mM EDTA, resuspended in serum-free culture medium (10,000 cells/mL), and plated onto the SAM substrates. After 2 hours, the substrates were placed in serum containing media and maintained at 37 °C in a humidified 5% CO₂ atmosphere.

Conclusions

We have developed a molecularly defined gradient that presents RGD peptide ligands for attached cell culture on model surfaces where the only interaction between cell and material is a ligand–receptor interaction. We have shown for the first time, that the ligand slope, ligand density and ligand affinity all direct cell migration behavior on biospecific molecular gradients. We also show how this strategy may be used to study the factors that influence and regulate cell polarity. The methodology presented here can be used with various cell lines and various ligands to study the interplay of gradient and ligand composition on adhesion, migration and cell-cell communication.^{42,43} The synthetic flexibility of the strategy also allows for the straightforward immobilization of a variety of biomolecules, different affinity ligands and small molecules that contain the oxyamine group.^{44,45} The gradient surfaces are designed at the molecular level and therefore provide exquisite control of the density and presentation of ligands for numerous cell based studies, assays and new biotechnological applications. This methodology combined with live cell fluorescence microscopy,^{46,47} nano-patterned surfaces and dynamic substrates^{26,48-52} will provide the generation of dynamic gradient

surfaces where the spatial and temporal control of cell migration may allow for internal and external insights into the subcellular nanoarchitecture that governs cell movement and cell-cell communication.⁵³⁻⁵⁷

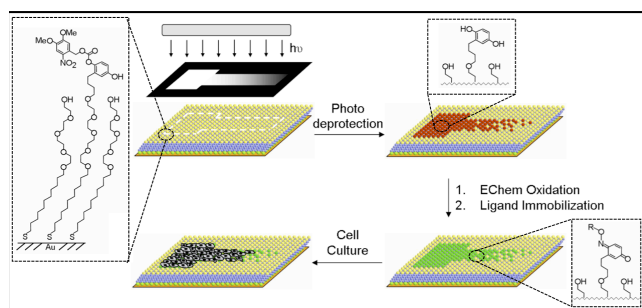
Notes and references

- ^a Department of Chemistry, The University of North Carolina at Chapel Hill, Chapel Hill, USA.
- ^b Department of Chemistry and Biology, Centre for Research in Biomolecular Interaction, Toronto, Canada. Fax: 416-736-5512; Tel: 416-736-2100 ext .77718; E-mail: chrchem@yorku.ca
- † Electronic Supplementary Information (ESI) available: See DOI: 10.1039/b000000x/
- A. J. Ridley, M. A. Schwartz, K. Burridge, R. A. Firtel, M. H. Ginsberg, G. Borisy, J. T. Parsons and A. R. Horwitz, *Science*, 2003, **302**, 1704-1709.
 - F. G. Giancotti and E. Ruoslahti, *Science*, 1999, **285**, 1028-1032.
 - D. J. Webb, J. T. Parsons and A. F. Horwitz, *Nat. Cell Biol.*, 2002, **4**, E97-E100.
 - D. A. Lauffenburger and A. F. Horwitz, *Cell*, 1996, **84**, 359-369.
 - S. P. Holly, M. K. Larson and L. V. Parise, *Exp. Cell Res.*, 2000, **261**, 69-74.
 - S. B. Carter, *Nature*, 1967, **213**, 256-260.
 - J. T. Smith, J. T. Elkin and W. M. Reichert, *Exp. Cell Res.* 2006, **312**, 2424-2432.
 - S. A. DeLong, J. J. Moon and J. L. West, *Biomaterials*, 2005, **26**, 3227-3234.
 - J. Y. Wong, A. Velasco, P. Rajagopalan and Q. Pham, *Langmuir*, 2004, **19**, 1908-1913.
 - D. W. Jiang, X. Y. Huang, F. Qiu, C. P. Luo and L. L. Huang, *Macromolecules*, 2010, **43**, 71-76.
 - I. Y. Tsai, M. Kimura and T. P. Russel, *Langmuir*, 2004, **20**, 5952-5957.
 - U. Hersel, C. Dahmen and H. Kessler, *Biomaterials*, 2003, **24**, 4385-4415.
 - J. H. Lee, J. W. Lee, G. Khang and H. B. Lee, *Biomaterials*, 1997, **18**, 351-358.
 - J. Pei, H. Hall and N. D. Spencer, *Biomaterials*, 2011, **32**, 8968-8978.
 - R. C. Gunawan, J. Silvestre, H. R. Gaskins, P. J. A. Kenis and D. E. Leckband, *Langmuir*, 2006, **22**, 4250-4258.
 - S. K. W. Dertinger, X. Y. Jaing, Z. Y. Li, V. N. Murthy and G. M. Whitesides, *Proc. Natl. Acad. Sci. U.S.A.*, 2002, **99**, 12542-12547.
 - B. P. Harris, J. K. Kutty, E. W. Fritz, C. K. Webb, K. J. L. Burg and A. T. Metters, *Langmuir*, 2006, **22**, 4467-4471.
 - C. B. Herbert, T. L. McLernon, C. L. Hypolite, D. N. Adams, L. Pikus, C. C. Huang, G. B. Fields, P. C. Letourneau, M. D. Distefano and W. S. Hu, *Chem. Biol.*, 1997, **4**, 731-737.
 - M. Mayer, J. Yang, I. Gitlin, D. H. Gracias and G. M. Whitesides, *Proteomics*, 2004, **4**, 2366-2376.
 - A. M. Bowen, J. A. Ritchey, J. S. Moore and R. G. Nuzzo, *Small*, 2011, **7**, 3350-3362.
 - B. Polyak, I. Fishbein, M. Chorny, I. Alferiev, D. Williams, B. Yellen, G. Friedman and R. J. Levy, *Proc. Natl. Acad. Sci. U.S.A.*, 2008, **105**, 698-703.
 - M. Iwasaka, K. Yamamoto, J. Ando and S. Ueno, *J. Appl. Phys.*, 2003, **93**, 6715-6717.
 - Q. Wang and P. W. Bohn, *Thin Solid Films*, 2006, **513**, 338-346.
 - S. T. Plummer, Q. Wang, P. W. Bohn, R. Stockton and M. A. Schwartz, *Langmuir*, 2003, **19**, 7528-7536.
 - E. W. L. Chan and M. Yousaf, *Mol. BioSyst.*, 2008, **4**, 746-753.
 - E. W. L. Chan, S. Park and M. N. Yousaf, *Angew. Chem. Int. Ed.*, 2008, **47**, 6267-6271.
 - W. S. Dillmore, M. N. Yousaf and M. Mrksich, *Langmuir*, 2004, **20**, 7223-7231.
 - M. Mrksich, *Chem. Soc. Rev.*, 2000, **29**, 267-273.
 - K. L. Prime and G. M. Whitesides, *Science*, 1991, **252**, 1164-1167.
 - E. W. L. Chan and M. N. Yousaf, *J. Am. Chem. Soc.*, 2006, **128**, 15542-15546.

- 31 E. W. L. Chan and M. N. Yousaf, *ChemPhysChem*, 2007, **8**, 1469-1472.
- 32 T. Horn, B. B. Lee, K. A. Dill and R. N. Zuckermann, *Bioconjugate Chem.*, 2004, **15**, 428-435.
- 33 D. H. Waldeck, A. P. Alivisatos and C. B. Harris, *Surf. Sci.*, 1985, **158**, 103-125.
- 34 E. Ruoslahti, *Annu. Rev. Cell Dev. Biol.*, 1996, **12**, 697-715.
- 35 D. D. Schlaepfer and C. R. Hauck, *Prog. Biophys. Mol. Biol.*, 1999, **71**, 435-478.
- 36 H.-B. Wang, M. Dembo, S. K. Hanks and Y. Wang, *Proc. Natl. Acad. Sci. U.S.A.*, 2001, **98**, 11295-11300.
- 37 S. K. Sastry and K. Burrige, *Exp. Cell Res.*, 2000, **261**, 25-36.
- 38 W. J. Nelson, *Nature*, 2003, **422**, 766-774.
- 39 M. Théry, V. Racine, M. Piel, A. Pépin, A. Dimitrov, Y. Chen, J.-B. Sibarita and M. Bornens, *Proc. Natl. Acad. Sci. U.S.A.*, 2006, **103**, 19771-19776.
- 40 R. T. Petty, H.-W. Li, J. H. Maduram, R. Ismagilov and M. Mrksich, *J. Am. Chem. Soc.*, 2007, **129**, 8966-8967.
- 41 A. D. Linstedt and H. P. Hauri, *Mol. Biol. Cell*, 1993, **4**, 679-693.
- 42 D. G. Barrett and M. N. Yousaf, *Angew. Chem. Int. Ed.*, 2007, **46**, 7437-7439.
- 43 W. Luo, E. W. L. Chan and M. N. Yousaf, *J. Am. Chem. Soc.*, 2011, **132**, 2614-2621.
- 44 B. M. Lamb, D. G. Barrett, N. P. Westcott and M. N. Yousaf, *Langmuir*, 2008, **24**, 8885-8889.
- 45 W. Luo, N. P. Westcott, A. Pulsipher and M. N. Yousaf, *Langmuir*, 2008, **24**, 13096-13101.
- 46 B. M. Lamb, N. P. Westcott and M. N. Yousaf, *ChemBioChem*, 2008, **9**, 2220-2224.
- 47 L. Hodgson, E. W. L. Chan, K. M. Hahn and M. N. Yousaf, *J. Am. Chem. Soc.*, 2007, **129**, 9264-9265.
- 48 D. K. Hoover, E. W. L. Chan and M. N. Yousaf, *J. Am. Chem. Soc.*, 2008, **130**, 3280-3281.
- 49 D. K. Hoover, E.-j. Lee, E. W. L. Chan and M. N. Yousaf, *ChemBioChem*, 2007, **8**, 1920-1923.
- 50 M. N. Yousaf, B. T. Houseman and M. Mrksich, *Angew. Chem. Int. Ed.*, 2001, **40**, 1093-1096.
- 51 J. Nakanishi, Y. Kikuchi, S. Inoue, K. Yamaguchi, T. Takarada and M. Maeda, *J. Am. Chem. Soc.*, 2007, **129**, 6694-6695.
- 52 W. Luo and M. N. Yousaf, *J. Am. Chem. Soc.*, 2011, **133**, 10780-10783.
- 53 S. Park and M. N. Yousaf, *Langmuir*, 2008, **24**, 6201-6207.
- 54 W. Luo, N. P. Westcott, A. Pulsipher and M. N. Yousaf, *Langmuir*, 2008, **24**, 13096-13101.
- 55 Y. Shimizu, H. Boehm, K. Yamaguchi, J.P. Spatz and J. Nakanishi, *PLOS ONE*, 2014, **9**, e91875.
- 56 W. Luo and M. N. Yousaf, *Chem. Comm.*, 2009, 1237-1239.
- 57 B.M. Lamb and M.N. Yousaf, *J. Am. Chem. Soc.*, 2011, **133**, 8870-8873.

50

Table of Content GRAPHIC



- 55 A patterned peptide gradient with control of slope and density is created for studies of directed cell polarization and migration.